DL-RMD: A geophysically constrained electromagnetic resistivity model database for deep learning applications

Muhammad Rizwan Asif[1,3,4], Nikolaj Foged[1,4], Thue Bording[1,2], Jakob Juul Larsen[3,4], and Anders Vest Christiansen[1,4]

[1]Hydro-Geophysics Group (HGG), Department of Geoscience, Aarhus University, Aarhus C, 8000, Denmark.
[2]Aarhus GeoInstruments, Åbyhøj, 8230, Denmark.
[3]Department of Electrical and Computer Engineering, Aarhus University, Aarhus N, 8200, Denmark.
[4]Aarhus University Centre for Water Technology (WATEC), Aarhus N, 8200, Denmark.

Correspondence to: Muhammad Rizwan Asif (rizwanasif@geo.au.dk, rizwansheikh123@hotmail.com)

Abstract. Deep learning algorithms have shown incredible potential in many applications. The success of these data-hungry methods is largely associated with the availability of large-scale data sets, as millions of observations are often required to achieve acceptable performance levels. Recently, there has been an increased interest in applying deep learning methods to geophysical applications where electromagnetic methods are used to map the subsurface geology by observing variations in the electrical resistivity of the subsurface materials. To date, there are no standardized datasets for electromagnetic methods, which hinders the progress, evaluation, benchmarking, and evolution of deep learning algorithms due to data inconsistency. Therefore, we present a large-scale electrical resistivity model database with a wide variety of geologically plausible and geophysically resolvable subsurface structures for the commonly deployed ground-based and airborne electromagnetic systems. Potentially, the presented database can be used to build surrogate models of well-known processes and to aid in labour intensive tasks. The geophysically constrained property of this database will not only achieve enhanced performance and improved generalization but, more importantly, it will incorporate consistency and credibility in deep learning models. We show the effectiveness of the presented database by surrogating the forward modelling process, and we urge the geophysical community interested in deep learning for electromagnetic methods to utilize the presented database. The dataset is publically available at https://doi.org/10.5281/zenodo.7260886 (Asif et al., 2022a).

1 Introduction

Recent years have witnessed the success of many deep learning (DL) applications. Although, DL emerged in 1982 in the form of neural networks (Hopfield, 1982), it started to gain attention in 2012 due to its notable performance for image classification tasks (Krizhevsky et al., 2017, 2012). Since then, it has been applied successfully to many applications including object

detection (Asif et al., 2019; Redmon et al., 2016; Ren et al., 2015), image super-resolution (Dong et al., 2016; Zhang et al.,
30 2018), speech recognition (Zhang et al., 2017), and stock market predictions (Pang et al., 2020). The revival of DL was mainly influenced by the availability of cheap computing resources, deeper network architectures and large-scale publically available datasets. Deeper network architectures and an increased number of samples in the training datasets are key factors for improved performance and better generalization of DL models (Wang et al., 2016).

Geophysics is a branch of earth sciences, and geophysical methods are often used to infer information about the subsurface
35 geology by mapping physical properties. The integration of neural networks in geophysics started several decades ago and has covered many domains of geophysics (Baan and Jutten, 2000; Dramsch, 2020) including seismic (Röth and Tarantola, 1994; Zhang et al., 2020), magneto-telluric (Conway et al., 2019; Liu et al., 2020; Zhang and Paulson, 1997) geo-mechanical (Feng and Seto, 1998; Khatibi and Aghajanpour, 2020), and electromagnetics (Birken and Poulton, 1999; Birken et al., 1999; Bording et al., 2021; Kwan et al., 2015; Poulton et al., 1992; Zhu et al., 2012). Interestingly, the last few years have seen a significant
40 increase of interest in applying DL to electromagnetic (EM) methods (see Table 1), where the artificially generated EM fields are used to map variations in the electrical resistivity properties of the subsurface. For more details regarding the EM methods, readers are referred to literature, e.g. (Kirsch, 2006). The increasing interest in applying DL to EM methods is mainly influenced by the increased ability of the EM methods to collect huge data sets in short amounts of time, which makes the subsequent processes extremely laborious and time consuming. Therefore, a DL method could be beneficial in surrogating
45 well-known EM processes, e.g. forward modelling where the propagation of the EM fields are simulated resulting in the forward responses (Xue et al., 2020), and inverse modelling (inversion) where the electrical resistivity properties of the subsurface are deduced from observed EM data (Zhdanov, 2015). DL methods can also assist with manual tasks, which may require considerable time when performed manually, such as anomaly detection in EM data. Further opportunities may lie in other tasks, e.g. data de-noising.

50 To apply a DL algorithm to EM methods for various applications, subsurface resistivity models and/or the corresponding EM responses are often required. To achieve optimal performance, a DL method should be trained on a large number of geologically realistic subsurface models. Evident from Table 1, the recently developed DL methods either uses subsurface resistivity models acquired from field data or generate the models randomly or in a pseudorandom manner for training. However, a method trained on random models, where the resistivity of each geological layer is chosen from a probability
55 distribution, would not result in optimal performance, as many of the training samples would be geologically unrealistic. A good solution is either to use resistivity models inverted from field data or pseudorandom resistivity models where the resistivity of the training models is based on some prior geological information to reflect various characteristics of field data (Bai et al., 2020). However, a DL method trained on such training samples would only be effective for specific geological conditions and would result in an unsatisfactory performance for significantly different geological settings (Bording et al.,

60   2021), as bias in the training data can affect generalizability substantially. Additionally, the unavailability of a standard benchmark database hinders the progress, evaluation, benchmarking, and evolution of DL algorithms due to data inconsistency (Bergen et al., 2019; Reichstein et al., 2019).

Table 1: Recent publications (2019-2021) of DL applications in EM which shows the number of training samples and type of training dataset (random, pseudorandom or field data)

Reference	No. of samples in training set	Training Observation type	Application
Wu et al. (2021a)	80,000	Pseudorandom resistivity models and forward responses	Inversion
Colombo et al. (2021a)	5,000	Pseudorandom resistivity models and forward responses	Inversion
Colombo et al. (2021b)	20,000	Random resistivity models and forward responses	Inversion
Wu et al. (2021b)	16,800	Forward responses of random resistivity models	De-noising
Bording et al. (2021)	93,500	Field data and inversion models	Forward modelling
Puzyrev and Swidinsky (2021)	5,12,000	Random resistivity models and forward responses	Inversion
Asif et al. (2021a)	100,000	Field data and inversion models	Forward modelling
Moghadas et al. (2020)	20,000	Random resistivity models and forward responses	Forward modelling
Bai et al. (2020)	12,000	Pseudorandom resistivity models and forward responses	Inversion
Li et al. (2020)	1,000,000	Pseudorandom resistivity models and forward responses	Inversion
Bang et al. (2020)	25,173	Pseudorandom resistivity models and forward responses	Inversion
Noh et al. (2020)	20,000	Random resistivity models and forward responses	Inversion
Moghadas (2020)	20,000	Random resistivity models and forward responses	Inversion
Colombo et al. (2020a)	2,35,620	Pseudorandom resistivity models and forward responses	Inversion
Colombo et al. (2020b)	88	Pseudorandom resistivity models and forward responses	Inversion
Lin et al. (2019)	2,400	Field data and inverted model forward responses	De-noising
Guo et al. (2019)	10,000	Pseudorandom resistivity models and forward responses	Inversion
Puzyrev (2019)	20,000	Pseudorandom resistivity models and forward responses	Inversion
Qin et al. (2019)	50,000	Random resistivity models and forward responses	Inversion

65   To have an inclusive DL solution for various applications in EM, we present a physics-driven large-scale model database (~1 million) of geologically plausible and EM resolvable 1-D sub-surface resistivity models spanning the resistivity range from 1 Ωm to 2000 Ωm and to a depth of 500 m. This model database is suitable for ground-based and airborne EM systems in a DL context. We use broad-banded von Kármán covariance functions to generate geologically constrained resistivity models. Geophysical constraints are imposed by calculating the EM forward data of the initial resistivity models followed by inversion

70   of the EM forward to obtain the final resistivity models. This allows us to create a comprehensive resistivity model database (RMD) that may not only improve performance and generalization, but would also incorporate consistency and reliability in the DL models. We believe that the presented RMD will be a valuable resource to accelerate the inter- and trans-disciplinary research of Earth and data sciences. The presented DL-RMD will also provide uniformity in training and benchmarking for DL methods in EM. Therefore, we urge the geophysical community interested in DL for EM methods to use the DL-RMD.

75   The rest of this paper is organized as follows: Section 2 describes the general methodology of generating the sub-surface resistivity models, while specific settings for the DL-RMD for the three EM system categories are specified in section 3. Section 4 provides details for training a DL method to surrogate the forward modelling problem and shows the effectiveness of the DL-RMD. Discussion, code and data availability, and concluding remarks are given in section 5, 6, and 7 respectively.

2 Methodology

80   Geological processes do not result in random structures, nor are the subsurface resistivity structures random, as some spatial correlation is generally present (Tacher et al., 2006). Therefore, it is reasonable that the training of a DL method is based on subsurface structures that are geologically plausible and, in an EM context, over all resolvable by the EM method. Additionally, the scale of the resistivity structure in the models should reflect the resolution capability of the EM methods, as training a DL method to resolve structures that are not evident in the input data is not possible. EM methods are diffusive methods with

85   significantly decreasing resolution with depth and the electrical conductivity contrast plays an important role for the resolution capability; hence, a metric number for a given EM method's resolution capability and the depth of investigation can not be given.

       To obtain geologically realistic models, we use the broad-banded von Kármán covariance functions (Møller et al., 2001) to generate geologically plausible models (von Kármán models). The suite of von Kármán models consists of fine geological

90   structures and contain some resistivity variations and patterns that are unlikely to be resolved, due to the resolution limitation of the EM method. To replicate the resolution capability of the EM method, we generate EM forward responses of the initially over-detailed von Kármán models and invert these forward responses to obtain the final resistivity models. Since we aim at generating 1-D resistivity models, we are only concerned about the resistivity (ρ) variations in the vertical direction (z) from surface to some depth in our model generation.

95   Initially, we base the spatial variation character of $(z, \log_{10}(\rho))$ for our von Kármán models on the broad-banded von Kármán covariance functions (Christiansen and Auken, 2003; Møller et al., 2001).

$$C(z, A, v) = A^2 C_0 \left(\frac{z}{L}\right)^v K_v \left(\frac{z}{L}\right),$$ (1)

       where A becomes the amplitude of the logarithmic resistivity, C_0 is a scaling constant, z the spatial (vertical) distance, L characterizes the maximum correlation length accounted for, and K_v is the modified Bessel function of second kind and order

100   v. In the model generation, L is fixed to a high number (1800 m) which gives us strong correlation for $z<<L$ (Maurer et al., 1998). By using combinations of v, C_0, and resistivity, and compiling several realizations of the stochastic von Kármán process, we generate a variety of resistivity models on multiple scales. Table 2 summarizes the L, v, C_0, and resistivity values used.

4

Table 2: Parameters used in all combinations to generate the initial von Kármán resistivity models.

Parameter	Values
Resistivity	1 to 2000 Ωm, log spaced, 20 values per decade
L	Fixed: 1800 m
v	[0.6, 0.7, 0.8, 0.9, 1.0]
C_0	[0.5, 1, 2, 4]
# sharp boundaries	[1, 2, 3, 4, 5]

Examples of this are shown in Figure 1(a-c) where the von Kármán models (in black curves) are generated with a combination of the extreme values of v, C_0 for an initial resistivity value of 30 Ωm. Low v and high C_0 produce models with fine and large-scale variations (Figure 1a), while high v and high C_0 values produce a relatively smooth model (Figure 1b) but still with resistivity variations spanning 2-3 decades of resistivity. The combination of low v and C_0 values ensure that the simple and close to half-space models are also represented (Figure 1c).

Sharp layering in the subsurface is plausible, and large resistivity amplitudes and short correlation lengths in the von Kármán functions will form layering in the models. To include more models with a sharp layering, we stitch 2-6 randomly selected depth intervals of the initially generated von Kármán models from a uniform distribution. An example of a stitched model is shown in Figure 1(d). These stitched models also ensure that different combinations of v, C_0, are represented within one model.
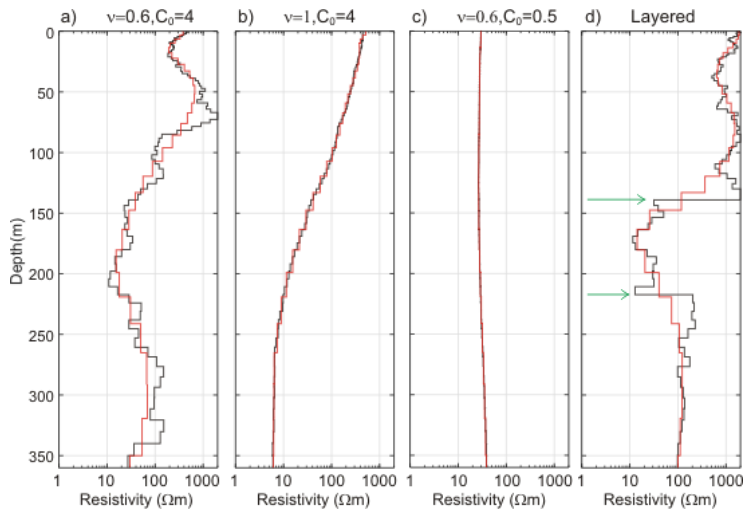

Figure 1: Examples of von Kármán models and the result after the forward and inversion process, where black curves shows von Kármán models (re-discretized to 90 layer) and the red curve shows the final model. (a-c) for the combination of v, C_0 stated in the title, (d) a stitched layered model (green arrows marks the imposed sharp layer boundaries). The red curves show the obtained model from inversion of the forward response of the black model.

Prior to the EM forward calculation, the von Kármán models are re-discretized to 90-layers for faster forward computation and easier handling. The top layer thickness and depth to the last layer boundary for the re-discretized layers have been detailed

5

120 in Table 3 for three generic EM systems with different depths of investigations (see Section 3 for further details). For the forward calculation, the geometric mean of the last 5 meters of the re-discretized von Kármán models is assigned to the last model layer that continues to infinity depth. In order to avoid making assumptions on the acquisition conditions, specific instrument setups, etc., the calculated forward data are pragmatically assigned a uniform uncertainty of 5% to take noise into account and is inverted with a 30-layer model with a minimum structure (smooth) regularization scheme (Viezzoli et al., 2008).

125 The layer thicknesses for the 30-layer models are fixed and have also been listed in Table 3. The red model curves in Figure 1 are the resistivity models after the forward and inversion process, and are the models that enter the DL-RMD. As seen from Figure 1, the von Kármán models hold structures that are not resolved by the inverted resistivity models, so the models obtained after the forward and inversion process result in structures resolvable by the EM method. A total of ~95% of the inverted resistivity models explain (fit) the forward data within the assumed data uncertainty. In other words, the inverted models are

130 explaining the more complex von Kármán models to a very high degree.

The forward and inverse modelling is carried out for three different generic time-domain EM (TEM) systems spanning different depth ranges using the AarhusInv modelling code (Auken et al., 2015). The specific DL-RMD settings for different TEM systems are summarized in section 3.

3 Deep learning resistivity model database (DL-RMD)

135 EM systems for subsurface exploration have existed since the 1950s, and nowadays a large variety of airborne and ground-based time-domain electromagnetic (TEM) and frequency-domain electromagnetic (FEM) systems exist. Both TEM and FEM methods map the electrical resistivity of the subsurface by inducing EM fields. TEM methods record the decay of the secondary EM-field in the absence of the transmitted EM-field in the time-domain, while FEM methods record the secondary EM-field in the frequency-domain in the presence of the transmitted EM-field (Christiansen et al., 2006). TEM and FEM methods also

140 differ in resolution and depth of investigation, depending on the TEM-system configuration, e.g. transmitter turn-off time, transmitter moment, airborne/ground-based. For the DL-RMD to be compatible for different TEM systems, we have compiled three model databases with ~1 million models in each for three generic TEM-systems with a different depth of investigation as their primary differences. We refer to the three DL-RMD as *shallow, intermediate*, and *deep*, with the acronyms S-RMD, I-RMD, D-RMD respectively. S-RMD mimics a shallow focusing ground based TEM system, initiated by a short transmitter

145 turn-off time. For S-RMD, the models are discretized down to 125 m with a top layer thickness of 0.5 m. I-RMD and D-RMD mimics airborne TEM with different depth of investigations, hence discretized down to a depth of 350 and 500 m and with a top layer thickness of 3 and 5 m respectively. The calculation of depth of investigation follows Christiansen and Auken (2012).

The model discretization for three DL-RMD for the initial von Kármán models and for the final resistivity models entering the RMD are summarized in Table 3. Table 3 also holds the key specifications of the three generic TEM systems. The settings for

150   the generation of the von Kármán models have been specified in Table 2 and are common for the three DL-RMD. Each of the
three DL-RMD holds ~1 million models spanning the resistivity interval 1-2000 Ωm, where 1/6 of the models originate from
the initially generated von Kármán models and 5/6 of the models come from the stitched layered von Kármán models.

Table 3: Model discretization and key specifications of the generic TEM systems for three resistivity model databases. The generic TEM system are all central loop configurations. *Gate start/end times has zero-time reference at begin of turn-off time.

Type	Parameter	S-RMD	I-RMD	D-RMD
von Kármán models	Max depth (m)	125	355	505 m
	Discretization (m)	0.1	0.1	0.1
	Re-discretization (m)	0.2-120 m, 90 layer log-spaced	1-350 m, 90 layer log-spaced	2-500 m, 90 layer log-spaced
Database resistivity models	Model Discretization	0.5-120 m, 30 layer log-spaced	3-350 m, 30 layer log-spaced	5-500 m, 30 layer log-spaced
Generic TEM configuration	Turn off time (µs)	4	12	40
	*Gate time start (µs)	5	13	50
	*Gate time end (ms)	1	10	32
	Modelling height (m)	0 – Ground-based	40 - Airborne	40 - Airborne

155   Some insights on the three DL-RMD are given in Figure 2, where Figure 2(a-c) shows the layer resistivity distribution of the
three DL-RMD. The resistivity distributions of the von Kármán models were generated uniformly, but the forward and
inversion process makes the resistivity distribution slightly skewed towards the lower resistivity end, due to the lower
sensitivity/resolution in the high resistivity end for the EM method (Christiansen et al., 2006; Jørgensen et al., 2005). The
larger start and end bins compared to the neighboring bins in Figure 2(a-c) are due to the 1 Ωm and 2000 Ωm resistivity
160   truncation. The estimated depths of investigation for the three DL-RMD are shown in Figure 2(d-f). We observe that
approximately 70% of the models have depth of investigation less than the bottom to last layer boundary of the given DL-
RMD. Especially, a thick conductive layer near the surface will significantly limit the depth of investigation for a given TEM
configuration. The uneven and in some cases limited depth of investigation does not pose a problem for a deep learning
algorithm, as the EM method will compromise a similar depth of investigation limitation for the given resistivity model (see
165   discussion section for more details).

7
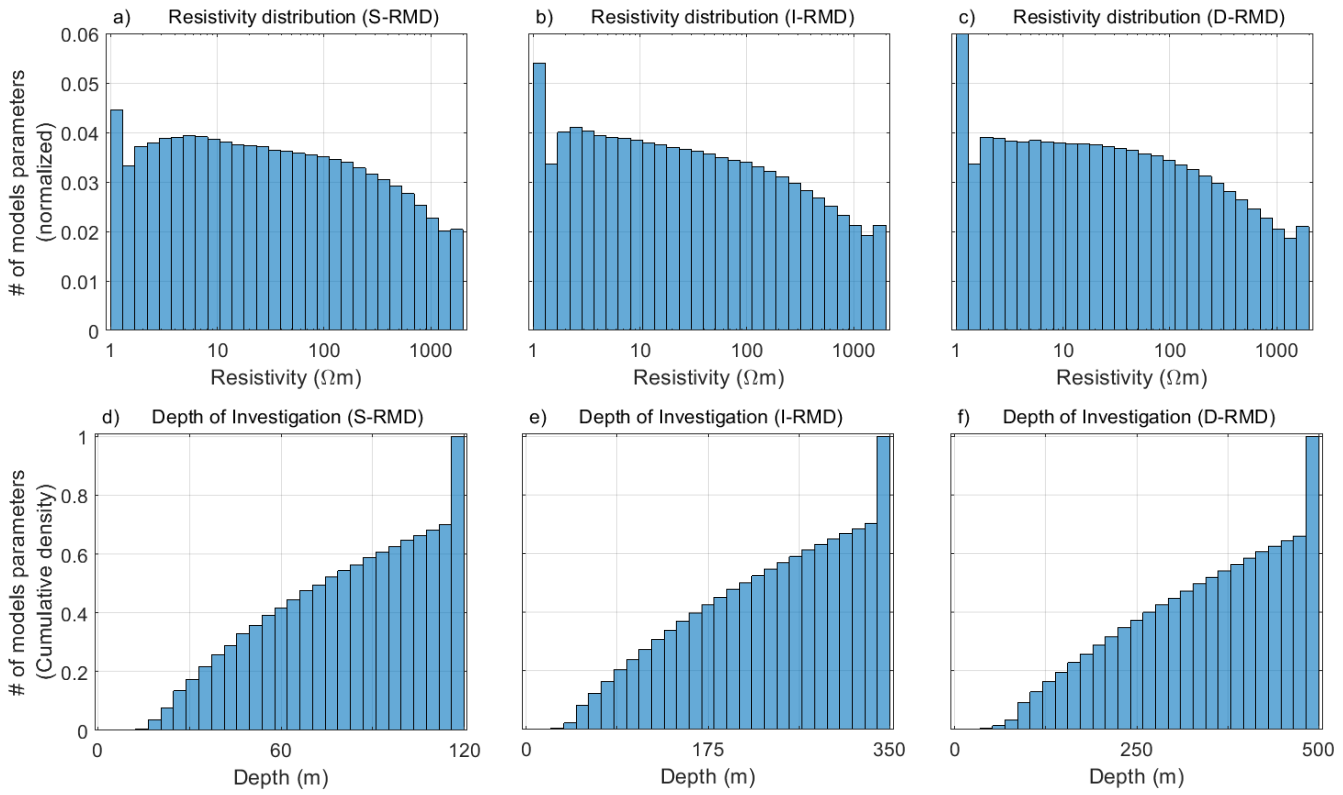
Figure 2: Statistical insights on the DL-RMD. (a-c) Resistivity distribution of the S-RMD, I-RMD, and D-RMD respectively. (d-f) Distribution of depth of investigation of models in the S-RMD, I-RMD, and D-RMD respectively, plotted as cumulative sum.

4 Example of an EM application using DL-RMD

EM methods can benefit from the presented DL-RMD in many ways. For example, the DL-RMD can be used to surrogate the computationally expensive numerical forward modelling by using a computationally efficient DL method, which would speed up the whole inversion process. It can also be used to develop a DL algorithm to replace the calculation of the partial derivatives in deterministic inversion methods, where the subsurface resistivity model is updated iteratively by using the partial derivatives of the model parameters. Detecting anomalies in the EM data by using a DL approach using the DL-RMD can significantly speed-up the EM data processing and limit the involvement of human-centric manual workflows. Additionally, EM data de-noising also becomes plausible.

As an example in this paper, we use the DL-RMD to surrogate the forward modelling problem for a ground-based TEM system using a fast DL method, since a significant number of forward calculations are required during the inversion process, when either deterministic or stochastic inversion methods are used. By replacing the computationally expensive numerical forward

8

modelling approach, the whole inversion process may be accelerated without further modification to a standard inversion workflow (Asif et al., 2021b). However, it is crucial that the performance of the DL method balances the numerical precision and increased speed of computation. If the prediction accuracy is not sufficiently high, the application in an inversion framework may result in spurious subsurface features and erroneous geological interpretations of the geophysical EM mapping
185   results.

4.1 Deep learning (DL) setup

We design the surrogate model for the tTEM system (Auken et al., 2018). The tTEM system is a ground-based towed TEM system with a maximum depth of investigation of 120 m based on the data time interval from ~5 µs to ~1 ms, which matches the specification of S-RMD, therefore, we use it to train our DL method.

190   The input to the DL algorithm becomes the 30-layer resistivity model $\mathbf{m}$ in S-RMD, where the layer thickness of each resistivity layer is fixed. The target outputs are the numerical TEM forward responses, i.e. dB/dt, for the corresponding inputs. A standard EM modelling code (Auken et al., 2015) is used to generate the TEM forward responses for the resistivity models $\mathbf{m}$ with fixed layer thicknesses. We generate the responses from ~1 ns to ~10 ms by exponentially increasing gate-widths sampled at 14 gates/decade.

195   Prior to the training of a DL method, inputs and the corresponding target outputs are normalized. Each resistivity model $\mathbf{m}$ is normalized, where the logarithmic variations in the model parameters can take both positive and negative values.

$$\mathbf{m}_n = \log_{10}(\mathbf{m}) - \frac{\mu[\log_{10}(m_{max}) + \log_{10}(m_{min})]}{2},$$ (2)

where m_{min} and m_{max} are the minimum and maximum resistivity values in the training data set of S-RMD, and μ is the mean.

The target outputs, i.e. dB/dt, are normalized by:

200   $$\frac{dB_n}{dt} = \frac{dB/dt - \mu[dB/dt])}{\sigma[dB/dt]},$$ (3)

where μ is the mean and σ is the standard deviation of each data point in the training data set.

We use a simple DL method where a fully-connected feed-forward neural network is utilized with two hidden layers, each having 384 neurons. The hyperbolic tangent function is used as an activation function between the hidden layers, and the full-batch scaled conjugate algorithm is used for backpropagation. The loss function for training is the sum of squared errors with
205   a regularization term consisting of the mean of sum of squares of the network weights and biases. The network configuration

9

used here is based on our previous results (Asif et al., 2021b; Asif et al., 2022b). We also apply an early stopping criterion to ensure that the training stops when the validation loss starts to increase. The validation set for the early stopping criteria comprises of 70,000 models from S-RMD, which are excluded from the training set. Once the network is trained, it can be used for evaluation purposes. The evaluation metric for our baselines is the percentage relative error, RL_P, defined in Eq. (3),
210 which effectively deals with the large dynamic range and patterns of TEM data.

$$RL_P = \frac{\left(\frac{d\mathbf{B}}{dt}\right)_{DL} - \left(\frac{d\mathbf{B}}{dt}\right)_N}{\left(\frac{d\mathbf{B}}{dt}\right)_N} \times 100\% \, , \tag{3}$$

where $\left(\frac{d\mathbf{B}}{dt}\right)_{DL}$ is the output of the DL method and $\left(\frac{d\mathbf{B}}{dt}\right)_N$ is the numerically computed forward response.

4.2 Surrogate forward modelling results

To test the performance of our DL method trained on S-RMD, we use 697 resistivity models inverted from field data from a
215 survey conducted in Søften, a region in Denmark. The data processing and inversion of the field data follows the method developed by Auken et al. (2018), which covers averaging, anomaly detection, manual inspection, etc. on the data. The minimum and maximum resistivity values in the test dataset are 3.9 Ωm and 127.1 Ωm respectively. The forward responses of the field inverted resistivity models are calculated numerically to compare them with the output of our DL method. Since the output of our DL algorithm is the normalized forward response, it is de-normalized to raw data values by manipulating Eq.
220 (3). For a relative comparison, we train another DL network with the same configuration using the initial von Kármán resistivity models. The comparison to the initial von Kármán resistivity models also allows us to examine the effect of the *forward/inversion* process, as described in section 2, in the generation of the DL-RMD. We also train an additional network using the random resistivity models similar to several DL studies (Colombo et al., 2021b; Moghadas, 2020; Moghadas et al., 2020; Noh et al., 2020; Puzyrev and Swidinsky, 2021; Qin et al., 2019; Wu et al., 2021b) as mentioned in Table 1. To have
225 the same level of complexity, the number of layers, depth discretization and the number of random resistivity models are kept the same as used to train other two networks for a fair comparison, and the resistivity of each layer is chosen randomly from a log-uniform distribution to take into account the non-linearity of the forward responses with the resistivity values. As such, a resistivity change from 1 Ωm to 10 Ωm would affect the forward data more than a change from 100 Ωm to 110 Ωm (Asif et al., 2021a).

230 Figure 3 shows the performance comparison of the trained networks based on the evaluation metric in Eq. (3) against the forward responses of 697 resistivity models from the Søften survey. Figure 3(a) shows the distribution of RL_P of the DL network trained on S-RMD. We also show the accuracy performance of the DL networks trained on von Kármán and the random resistivity models. It is evident that the network trained on S-RMD results in lower errors as compared to the network trained on von Kármán resistivity models. On the other hand, the network trained on random resistivity models results in a

235   poor accuracy performance. In quantitative terms, 71% of the data points are evaluated to be within half a percent relative error for the network trained on S-RMD. In comparison to S-RMD, the network trained on von Kármán resistivity models results in 65% of data points within half a percent relative error. The network trained on random resistivity models performs the worst and only 34% of the data points are calculated to be within half a percent relative error.

a) Performance comparison (error distribution)   b) Performance comparison (cumulative density)
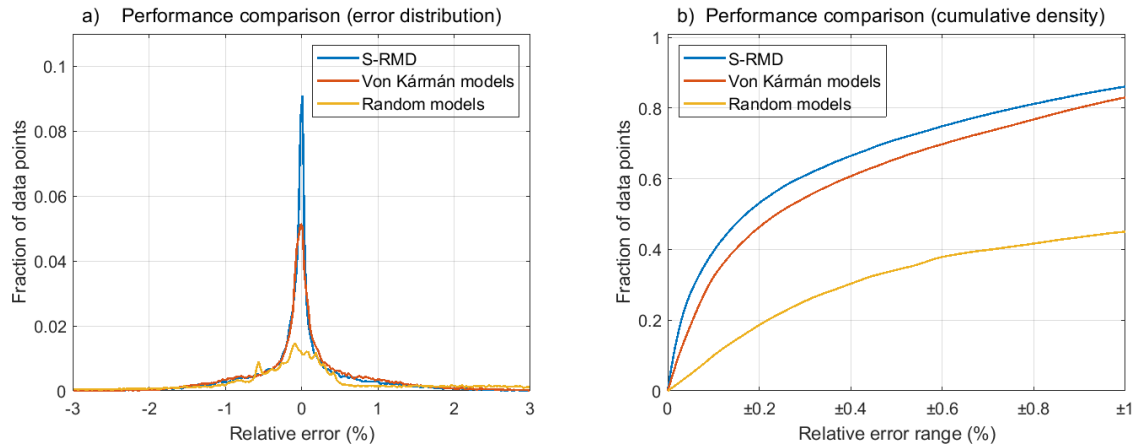
240   **Figure 3: Performance of the networks trained on S-RMD, von Kármán and random resistivity models. (a) RL$_P$ distribution. (b) Cumulative distribution of RL$_P$.**

We also show the cumulative distribution of the RL$_P$ for the networks trained on S-RMD, von Kármán and random models in Figure 3(b). A maximum of 9% improvement in accuracy is achieved for the network trained on the S-RMD as compared to the von Kármán models. In comparison to the network trained on random resistivity models, an improvement of 43% is
245   achieved when S-RMD is used for training. The increase in accuracy is achieved only by using an appropriate dataset for training. The prediction accuracy can be improved with different data pre-processing, network configurations, loss functions, etc. while using the same training dataset to allow consistency in benchmarking of DL algorithms. It is also important that a balance between the prediction performance and computational efficiency is maintained. As such, the computational time for the forward pass of the proposed network configuration can serve as a baseline for time comparison.

250   Figure 4 shows a visual comparison of a numerical forward response against the forward response from the trained networks for one of the resistivity models from the Søften survey. It is evident from Figure 4 that the forward response from the network trained on S-RMD is the most accurate and has a maximum relative error of 1.4% for the data point at ~72 μs (see Figure 4a). The highest error for the forward response from the network trained on von Kármán models is observed to be 2.5% for the data point at ~160 μs as shown in Figure 4(b). The forward response from the network trained on random models results in
255   the worst accuracy performance and results in a maximum error of 22.3% for the data point at 100 μs (see Figure 4c).
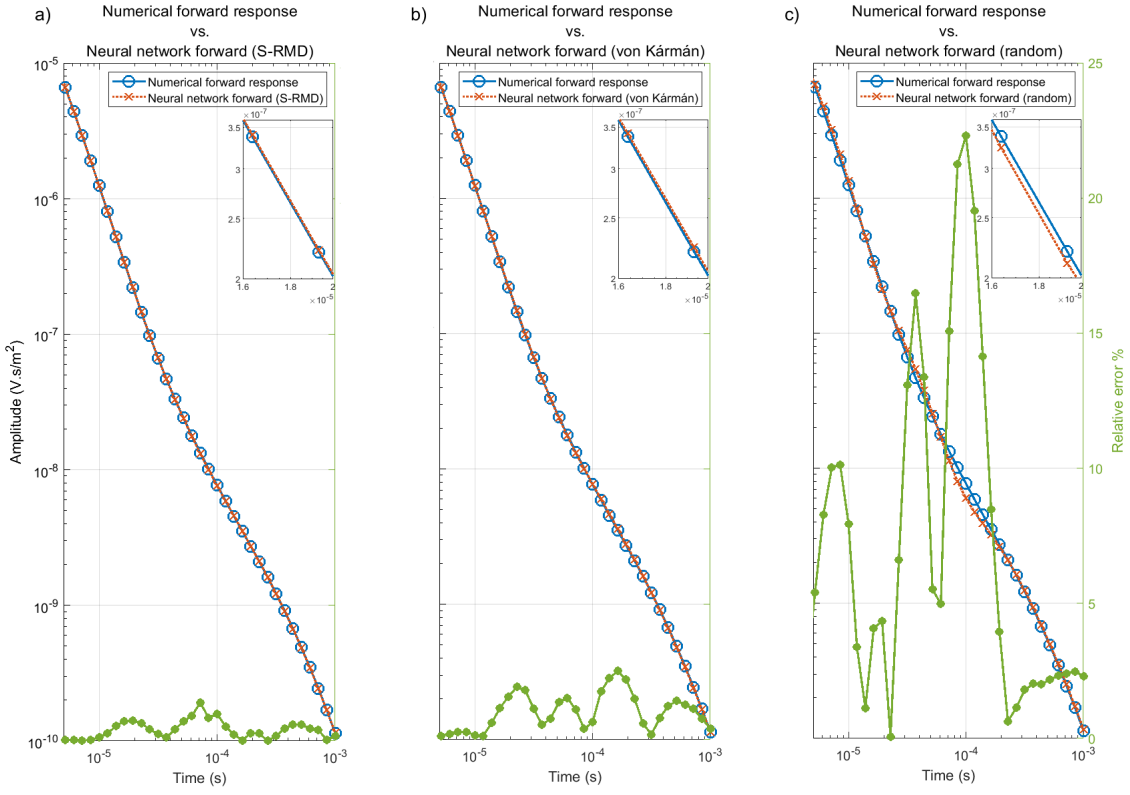
Figure 4: Comparison of performance of the networks trained on S-RMD, von Kármán and random resistivity models with a numerical forward response from the test set. The forward responses are shown only within the time range of tTEM data, and the inset shows the forward response from 16 µs to 20 µs (a) Numerical forward response vs. the forward response from the network trained on S-RMD. (b) Numerical forward response vs. the forward response from the network trained on von Kármán models. (c) Numerical forward response vs. the forward response from the network trained on random resistivity models.

5 Discussion

The network trained on random resistivity models results in a poor accuracy performance as many of the resistivity models in the training dataset are geologically unrealistic. The complex unrealistic resistivity structures in the randomly generated training models would result in forward responses similar to the ones obtained from simpler resistivity models, which further decreases the quality of the training dataset. The von Kármán models may be considered as pseudorandom resistivity models where the resistivity structure of the models have a geologically realistic nature as it considers multiple correlation lengths with stochastic nature resembling geological processes. Due to the geological nature of the von Kármán models, the network trained on such models results in a decent performance accuracy. However, the network trained on von Kármán models has a lower accuracy performance as compared to the network trained on S-RMD, where the resolution capability of the EM method has been taken into account resulting in resistivity structures resolvable by the EM method.

The resolution capability and the depth of investigation for a given TEM system strongly depends on the underlying resistivity model. Therefore, stating a single depth of investigation value for a given TEM system is not appropriate. A single exploration depth, depth of investigation, or a similar value stated by the instrument manufacturers will often be an optimistic one. For

275   TEM systems with short transmitter current turn-off, the early time data points provide the near surface resolution, while the late time data points strongly control the depth of investigation for a given resistivity model. The transmitter moment and the background noise level also influence the depth of investigation, but these factors are not considered in our case, since we have assumed a uniform data uncertainty in the forward and inversion process. The three DL-RMD span different TEM systems and resolutions. Therefore, for a particular TEM system, one should pick the DL-RMD that has a similar resolution as the

280   underlying generic TEM system. This is best evaluated by matching the time interval of the data for the particular TEM system to the data time interval (data time start/end in Table 3) for the generic TEM system.

In Table 4, we list some examples of the compatibility of our DL-RMD with some well-known TEM systems. Despite the I-RMD and D-RMD being compiled for a generic airborne-system, the I-RMD and D-RMD are also appropriate for ground-based TEM systems since the simulated flight altitude of 40 m does not lead to a drastic change in the vertical resolution.

285   **Table 4: Examples of DL-RMD compatibility for some TEM systems.**

System	Resistivity model database		
	S-RMD	I-RMD	D-RMD
EQUATOR (Karshakov et al., 2017)	✓		
tTEM (Auken et al., 2018)	✓		
MEGATEM (Smith et al., 2003)		✓	
AEROTEM (Balch et al., 2003)		✓	
SkyTEM (Sørensen and Auken, 2004)		✓	✓
GEOTEM (Smith, 2010)		✓	✓
SPECTREM^{PLUS} (Leggatt et al., 2000)			✓

Since FEM and TEM systems follow the same laws of physics, the DL-RMD is also applicable for many FEM systems, despite the generic EM system in the forward/inversion process mimicking the TEM systems. In general, the FEM systems have a shallower depth of investigation than that of the TEM systems, hence, the S-RMD is best suited for FEM systems. An alternative to the DL-RMD is to generate the resistivity model realizations by following the described methodology for the

290   specific EM system by using the von Kármán models provided (Asif et al., 2022a). This will ensure a 100% match between resolution, depth of investigation, etc. in the model domain compared to sensitivity in the EM data domain.

Despite the initial von Kármán models with super-imposed layering, the resistivity models in the DL-RMD have a pronounced vertical smooth behavior due to the minimum structure (smooth) regularization scheme (Viezzoli et al., 2008) used in the inversion phase. Applying another regularization scheme in the inversion phase, e.g., the minimum support norm (Vignoli et al., 2015) or using a few layer model discretization with no vertical regularization, one could compile a resistivity model database with different appearances. For our DL-RMD, we chose the minimum structure regularization scheme, since it is commonly used for inverting airborne and ground-based EM data. It is important to point out that a TEM data curve itself does not hold information about whether subsurface boundaries are smooth or sharp. As such, both the smooth and a sharp-layered model will explain the recorded data equally well in most cases. With our approach of compiling resistivity models, we have tried to avoid the inclusion of models with different smooth/sharp behavior that result in identical or close to identical forward data responses (equivalent models).

The DL-RMD is generated in the resistivity range of 1-2000 Ωm which covers most of the geological settings, taking into account the EM mapping capability in the high resistivity range. The resistivity limit of 2000 Ωm was chosen since EM methods have no or very little sensitivity in the high resistivity range, since high resistivity materials (e.g. granite, basalt, glacier ice, etc.) produce an EM signal below the detection level. Despite the 2000 Ωm limit, the resistivity distribution of the models in the DL-RMD is slightly skewed towards lower resistivities due to the limited sensitivity of the EM method to high resistivity values. A slight bias towards lower resistivity values may affect the performance of a DL method for high resistive models. However, even if an actual subsurface model is represented by a high resistive model, it is expected that any TEM method would have difficulty in resolving such a model. The RMD also has a limitation in the low resistivity end, e.g., in settings with seawater and saltwater intrusion, which may result in subsurface materials with resistivity values below 1 Ωm.

Since the 1-D models of the DL-RMD hold resistivity variations in one dimension (vertical) only, they cannot be used for calculating 2-D or 3-D EM-responses. Examples of geological settings where a 1-D approach would be inappropriate include steep dipping geological structures, thin sheets mineralization, mapping close to or on the shoreline, or areas with strong topographical variations. However, one could apply the same methodology to compile a 2-D or 3-D resistivity database. In this case, one would generate the initial von Kármán models as 2-D section or 3-D volumes, and use a 2-D or 3-D forward and inversion process, which of course would be much more computationally expensive compared to the 1-D case. However, the DL-RMD provided in this study opens the possibility of exploring more deep learning frameworks, and have reliability and consistency in performance comparisons for 1-D models.

6 Code and data availability

320 The DL-RMD is freely available at https://doi.org/10.5281/zenodo.7260886 (Asif et al., 2022a) and a ready to run demo code in Python Jupyter Notebook that uses the network trained on S-RMD and reproduces the results of this paper is available at https://github.com/rizwanasif/DL-RMD.

The EM modelling code "AarhusInv" (Auken et al., 2015) used to generate EM forward responses in this study is freely available to researchers for non-commercial activities. The details are available at https://hgg.au.dk/software/aarhusinv.

325 **7 Conclusion**

We have presented a methodology for compiling a geophysically constrained subsurface resistivity model database for applications related to electromagnetic data. We generated three 1-D resistivity databases, discretized to depths of 120 m, 350 m, and 500 m in the resistivity range of 1-2000 Ωm, hence covering various ground-based and airborne frequency-domain and time-domain electromagnetic systems and most of the geological settings. The upper resistivity limit of the model database is

330 satisfactory as the electromagnetic methods have limitations for high resistivity, however, the model database has limitations in the low resistivity for subsurface materials below 1 Ωm that may occur in some cases. Additionally, the database holds 1-D models and therefore inherits the limitations of 1-D electromagnetic modelling.

The example included using the proposed resistivity model database and deep learning for surrogating TEM forward modelling showing that high accuracy can be obtained with our resistivity model database. Furthermore, the example shows that the

335 forward/inversion steps in the generation of the database lead to a significantly increased performance in the forward modelling.

Despite some limitations, the generated resistivity model database is a well-organized database, which empowers the geoscience community to have consistency and credibility in the development of deep learning methods for many tasks including surrogating forward modelling, inverse modelling, data de-noising, automatic data processing, etc. Therefore, we

340 urge the geophysical community to utilize the presented database to develop and investigate different network configurations, data pre-processing strategies, loss functions, etc. while using the presented model database to allow consistency in benchmarking deep learning algorithms. The resistivity model database has already proven valuable in significantly improving the accuracy of neural networks for the forward modelling of electromagnetic data.

References

Asif, M. R., Bording, T. S., Barfod, A. S., Grombacher, D. J., Maurya, P. K., Christiansen, A. V., Auken, E., and Larsen, J. J.: Effect of data pre-processing on the performance of neural networks for 1-D transient electromagnetic forward modelling, IEEE Access, 9, 34635-34646, 2021a.

350   Asif, M. R., Bording, T. S., Maurya, P. K., Zhang, B., Fiandaca, G., Grombacher, D. J., Christiansen, A. V., Auken, E., and Larsen, J. J.: A Neural Network-Based Hybrid Framework for Least-Squares Inversion of Transient Electromagnetic Data, IEEE Transactions on Geoscience and Remote Sensing, doi: 10.1109/TGRS.2021.3076121, 2021b.

Asif, M. R., Foged, N., Bording, T., Larsen, J. J., and Christiansen, A. V.: DL-RMD: A geophysically constrained electromagnetic resistivity model database for deep learning applications (Dataset). Zenodo, 2022a.

355   Asif, M. R., Foged, N., Maurya, P. K., Grombacher, D. J., Christiansen, A. V., Auken, E., and Larsen, J. J.: Integrating neural networks in least-squares inversion of airborne time-domain electromagnetic data, Geophysics, 87, 1-54, 2022b.

Asif, M. R., Qi, C., Wang, T., Fareed, M. S., and Khan, S.: License plate detection for multi-national vehicles–a generalized approach, Multimedia Tools and Applications, 78, 35585-35606, 2019.

360   Auken, E., Christiansen, A. V., Kirkegaard, C., Fiandaca, G., Schamper, C., Behroozmand, A. A., Binley, A., Nielsen, E., Effersø, F., and Christensen, N. B.: An overview of a highly versatile forward and stable inverse algorithm for airborne, ground-based and borehole electromagnetic and electric data, Exploration Geophysics, 46, 223-235, 2015.

Auken, E., Foged, N., Larsen, J. J., Lassen, K. V. T., Maurya, P. K., Dath, S. M., and Eiskjær, T. T.: tTEM—A towed transient electromagnetic system for detailed 3D imaging of the top 70 m of the subsurface, Geophysics, 84, E13-E22, 2018.

365   Baan, M. v. d. and Jutten, C.: Neural networks in geophysical applications, Geophysics, 65, 1032-1047, 2000.

Bai, P., Vignoli, G., Viezzoli, A., Nevalainen, J., and Vacca, G.: (Quasi-) Real-Time Inversion of Airborne Time-Domain Electromagnetic Data via Artificial Neural Network, Remote Sensing, 12, 3440, 2020.

Balch, S., Boyko, W., and Paterson, N.: The AeroTEM airborne electromagnetic system, The Leading Edge, 22, 562-566, 2003.

Bang, M., Oh, S., Noh, K., Seol, S. J., and Byun, J.: Imaging of subsurface orebody with airborne electromagnetic data using a recurrent
370   neural network. In: SEG Technical Program Expanded Abstracts 2020, Society of Exploration Geophysicists, 2020.

Bergen, K. J., Johnson, P. A., Maarten, V., and Beroza, G. C.: Machine learning for data-driven discovery in solid Earth geoscience, Science, 363, eaau0323, 2019.

Birken, R. A. and Poulton, M. M.: Neural Network Interpretation of High Frequency Electromagnetic Ellipticity Data Part II: Analyzing 3D Responses, Journal of Environmental Engineering Geophysics, 4, 149-165, 1999.

375   Birken, R. A., Poulton, M. M., and Lee, K. H.: Neural Network Interpretation of High Frequency Electromagnetic Ellipticity Data Part I: Understanding the Half-Space and Layered Earth Response, Journal of Environmental Engineering Geophysics, 4, 93-103, 1999.

Bording, T. S., Asif, M. R., Barfod, A. S., Larsen, J. J., Zhang, B., Grombacher, D. J., Christiansen, A. V., Engebretsen, K. W., Pedersen, J. B., Maurya, P. K., and Auken, E.: Machine learning based fast forward modelling of ground-based time-domain electromagnetic data, Journal of Applied Geophysics, 187, 104290, 2021.

380   Christiansen, A. V. and Auken, E.: A global measure for depth of investigation, Geophysics, 77, WB171-WB177, 2012.

Christiansen, A. V. and Auken, E.: Layered 2-D inversion of profile data, evaluated using stochastic models, ASEG Extended Abstracts, 2003, 1-8, 2003.

Christiansen, A. V., Auken, E., and Sørensen, K.: The transient electromagnetic method. In: Groundwater geophysics, Springer, 2006.

Colombo, D., Li, W., Rovetta, D., Sandoval-Curiel, E., and Turkoglu, E.: Physics-driven deep learning joint inversion. In: SEG Technical
385   Program Expanded Abstracts 2020, Society of Exploration Geophysicists, 2020a.

Colombo, D., Li, W., Sandoval-Curiel, E., and McNeice, G. W.: Electromagnetic reservoir monitoring with machine-learning inversion and fluid flow simulators, Fifth International Conference on Engineering Geophysics (ICEG), 167-170, 2020b.

Colombo, D., Turkoglu, E., Li, W., and Rovetta, D.: Coupled physics-deep learning inversion, Computers and Geosciences, 157, 104917, 2021a.

390   Colombo, D., Turkoglu, E., Li, W., Sandoval-Curiel, E., and Rovetta, D.: Physics-driven deep learning inversion with application to transient electromagnetics, Geophysics, 86, 1-65, 2021b.

Conway, D., Alexander, B., King, M., Heinson, G., and Kee, Y.: Inverting magnetotelluric responses in a three-dimensional earth using fast forward approximations based on artificial neural networks, Computers & Geosciences, 127, 44-52, 2019.

Dong, C., Loy, C. C., and Tang, X.: Accelerating the super-resolution convolutional neural network, European conference on computer vision, 391-407, 2016.

Dramsch, J. S.: 70 years of machine learning in geoscience in review, Advances in Geophysics, doi: 10.1016/bs.agph.2020.08.002. 2020.

Feng, X.-T. and Seto, M.: Neural network dynamic modelling of rock microfracturing sequences under triaxial compressive stress conditions, Tectonophysics, 292, 293-309, 1998.

Guo, R., Li, M., Fang, G., Yang, F., Xu, S., and Abubakar, A.: Application of supervised descent method to transient electromagnetic data inversion, Geophysics, 84, E225-E237, 2019.

Hopfield, J. J.: Neural networks and physical systems with emergent collective computational abilities, Proceedings of the national academy of sciences, 79, 2554-2558, 1982.

Jørgensen, F., Sandersen, P. B., Auken, E., Lykke-Andersen, H., and Sørensen, K.: Contributions to the geological mapping of Mors, Denmark–a study based on a large-scale TEM survey, Bulletin of the Geological Society of Denmark, 52, 53-75, 2005.

Karshakov, E. V., Podmogov, Y. G., Kertsman, V. M., and Moilanen, J.: Combined Frequency Domain and Time Domain Airborne Data for Environmental and Engineering Challenges, Journal of Environmental Engineering Geophysics, 22, 1-11, 2017.

Khatibi, S. and Aghajanpour, A.: Machine Learning: A Useful Tool in Geomechanical Studies, a Case Study from an Offshore Gas Field, Energies, 13, 3528, 2020.

Kirsch, R.: Groundwater geophysics: a tool for hydrogeology, Springer, 2006.

Krizhevsky, A., Sutskever, I., and Hinton, G. E.: Imagenet classification with deep convolutional neural networks, Communications of the ACM, 60, 84-90, 2017.

Krizhevsky, A., Sutskever, I., and Hinton, G. E.: ImageNet classification with deep convolutional neural networks, Advances in Neural Information Processing Systems, 25, 2012.

Kwan, K., Reford, S., Abdoul-Wahab, D. M., Pitcher, D. H., Bournas, N., Prikhodko, A., Plastow, G., and Legault, J. M.: Supervised neural network targeting and classification analysis of airborne EM, magnetic and gamma-ray spectrometry data for mineral exploration, ASEG Extended Abstracts, 2015, 1-5, 2015.

Leggatt, P. B., Klinkert, P. S., and Hage, T. B.: The Spectrem airborne electromagnetic system—Further developments, Geophysics, 65, 1976-1982, 2000.

Li, J., Liu, Y., Yin, C., Ren, X., and Su, Y.: Fast imaging of time-domain airborne EM data using deep learning technology, Geophysics, 85, 1-38, 2020.

Lin, F., Chen, K., Wang, X., Cao, H., Chen, D., and Chen, F.: Denoising stacked autoencoders for transient electromagnetic signal denoising, Nonlinear Processes in Geophysics, 26, 13-23, 2019.

Liu, W., Lü, Q., Yang, L., Lin, P., and Wang, Z.: Application of Sample-Compressed Neural Network and Adaptive-Clustering Algorithm for Magnetotelluric Inverse Modeling, IEEE Geoscience Remote Sensing Letters, 18, 2020.

Maurer, H., Holliger, K., and Boerner, D. E.: Stochastic regularization: Smoothness or similarity?, Geophysical Research Letters, 25, 2889-2892, 1998.

Moghadas, D.: One-dimensional deep learning inversion of electromagnetic induction data using convolutional neural network, Geophysical Journal International, 222, 247-259, 2020.

Moghadas, D., Behroozmand, A. A., and Christiansen, A. V.: Soil electrical conductivity imaging using a neural network-based forward solver: Applied to large-scale Bayesian electromagnetic inversion, Journal of Applied Geophysics, 176, 104012, 2020.

Møller, I., Jacobsen, B. H., and Christensen, N. B.: Rapid inversion of 2-D geoelectrical data by multichannel deconvolution, Geophysics, 66, 800-808, 2001.

Noh, K., Yoon, D., and Byun, J.: Imaging subsurface resistivity structure from airborne electromagnetic induction data using deep neural network, Exploration Geophysics, 51, 214-220, 2020.

Pang, X., Zhou, Y., Wang, P., Lin, W., and Chang, V.: An innovative neural network approach for stock market prediction, The Journal of Supercomputing, 76, 2098-2118, 2020.

Poulton, M. M., Sternberg, B. K., and Glass, C. E.: Location of subsurface targets in geophysical data using neural networks, Geophysics, 57, 1534-1544, 1992.

Puzyrev, V.: Deep learning electromagnetic inversion with convolutional neural networks, Geophysical Journal International, 218, 817-832, 2019.

Puzyrev, V. and Swidinsky, A.: Inversion of 1D frequency-and time-domain electromagnetic data with convolutional neural networks, Computers & Geosciences, 149, 104681, 2021.

Qin, S., Wang, Y., Tai, H.-M., Wang, H., Liao, X., and Fu, Z.: TEM apparent resistivity imaging for grounding grid detection using artificial neural network, IET Generation, Transmission, Distribution, 13, 3932-3940, 2019.

17

445   Redmon, J., Divvala, S., Girshick, R., and Farhadi, A.: You only look once: Unified, real-time object detection, Proceedings of the IEEE conference on computer vision and pattern recognition, 779-788, 2016.

Reichstein, M., Camps-Valls, G., Stevens, B., Jung, M., Denzler, J., and Carvalhais, N.: Deep learning and process understanding for data-driven Earth system science, Nature, 566, 195-204, 2019.

Ren, S., He, K., Girshick, R., and Sun, J.: Faster r-cnn: Towards real-time object detection with region proposal networks, Advances in
450   neural information processing systems, 91-99, 2015.

Röth, G. and Tarantola, A.: Neural networks and inversion of seismic data, Journal of Geophysical Research: Solid Earth, 99, 6753-6768, 1994.

Smith, R., Fountain, D., and Allard, M.: The MEGATEM fixed-wing transient EM system applied to mineral exploration: a discovery case history, First Break, 21, 2003.

455   Smith, R. S.: Airborne electromagnetic methods: Applications to minerals, water and hydrocarbon exploration, Canadian Society of Explortation Geophysics, 35, 2010.

Sørensen, K. I. and Auken, E.: SkyTEM-A new high-resolution helicopter transient electromagnetic system, Exploration Geophysics, 35, 191-199, 2004.

Tacher, L., Pomian-Srzednicki, I., and Parriaux, A.: Geological uncertainties associated with 3-D subsurface models, Computers and
460   Geosciences, 32, 212-221, 2006.

Viezzoli, A., Christiansen, A. V., Auken, E., and Sørensen, K.: Quasi-3D modeling of airborne TEM data by spatially constrained inversion, Geophysics, 73, F105-F113, 2008.

Vignoli, G., Fiandaca, G., Christiansen, A. V., Kirkegaard, C., and Auken, E.: Sharp spatially constrained inversion with applications to transient electromagnetic data, Geophysical Prospecting, 63, 243-255, 2015.

465   Wang, W., Zhang, M., Chen, G., Jagadish, H., Ooi, B. C., and Tan, K.-L.: Database meets deep learning: Challenges and opportunities, ACM SIGMOD Record, 45, 17-22, 2016.

Wu, S., Huang, Q., and Zhao, L.: Convolutional neural network inversion of airborne transient electromagnetic data, Geophysical Prospecting, 69, 1761-1772, 2021a.

Wu, S., Huang, Q., and Zhao, L.: De-noising of transient electromagnetic data based on the long short-term memory-autoencoder,
470   Geophysical Journal International, 224, 669-681, 2021b.

Xue, G., Li, H., He, Y., Xue, J., and Wu, X.: Development of the Inversion Method for Transient Electromagnetic Data, IEEE Access, 8, 146172-146181, 2020.

Zhang, R., Liu, Y., and Sun, H.: Physics-guided convolutional neural network (PhyCNN) for data-driven seismic response modeling, Engineering Structures, 215, 110704, 2020.

475   Zhang, Y. and Paulson, K.: Regularized hopfield neural networks and its application to one-dimensional inverse problem of magnetotelluric observations, Inverse Problems in Engineering, 5, 33-53, 1997.

Zhang, Y., Pezeshki, M., Brakel, P., Zhang, S., Bengio, C. L. Y., and Courville, A.: Towards end-to-end speech recognition with deep convolutional neural networks, arXiv preprint arXiv:.02720, 2017.

Zhang, Z., Qi, C., and Asif, M. R.: Investigation on Projection Space Pairs in Neighbor Embedding Algorithms, 2018, 125-128.

480   Zhdanov, M. S.: Inverse theory and applications in geophysics, Elsevier, 2015.

Zhu, K.-G., Ma, M.-Y., Che, H.-W., Yang, E.-W., Ji, Y.-J., Yu, S.-B., and Lin, J.: PC-based artificial neural network inversion for airborne time-domain electromagnetic data, Journal of Applied Geophysics, 9, 1-8, 2012.